ELSEVIER

Physics of the Earth and Planetary Interiors 99 (1997) 131–143

PHYSICS OF THE EARTH AND PLANETARY INTERIORS

Slabs, hotspots, cratons and mantle convection revealed from residual seismic tomography in the upper mantle

Lianxing Wen *, Don L. Anderson

Seismological Laboratory 252-21, California Institute of Technology, Pasadena, CA 91125, USA

Received 6 June 1995; revised 26 February 1996; accepted 5 March 1996

Abstract

To further investigate the fate of slabs, the structure of hotspots and the style of mantle convection, we calculate residual tomographic maps in the upper mantle by excluding from the tomography the first-order effects of conductive cooling of oceanic plates, deep cratonic 'roots', and cooling or partial melting associated with subducted lithosphere. No correlation is found between residual tomography in the upper mantle and the 30–130 Ma subduction. The good correlations between residual tomography in the transition zone (400–650 km) and 0–30 Ma subduction, at spherical harmonic degree $l = 2$ can be explained either by slab accumulation in the transition zone beneath some subduction zones or by the poor lateral resolution of seismic tomography. Hotspots correlate with the residual tomography in the shallow (100–400 km) and the lowermost mantle at degree $l = 2$. However, correlations of hotspots and seismic velocities in the middle mantle, and correlations between residual tomography at shallow depths and lowermost-mantle tomography are poor. Therefore the connection between residual tomography at shallow depths and seismic tomography in the lowermost mantle is not clear. Craton distribution correlates with distribution of hotspots and residual topography very well at degree $l = 6$. This might indicate that cratonic 'roots' may affect the locations of upwellings and thus modulate upper-mantle convection, or that the degree $l = 6$ could be intrinsic in upper-mantle convection, with cratons and and other near-surface features establishing the pattern.

1. Introduction

The relationship between subduction and seismic tomography has been studied extensively. Richards and Engebretson (1992) interpreted the good correlations between the large-scale seismic heterogeneity, averaged over the whole lower mantle, and subduction during the Cenozoic and Mesozoic as the result of the cooling effects of the subduction. Scrivner and Anderson (1992) correlated subduction positions since the breakup of Pangea with seismic tomography depth by depth throughout the whole mantle. They found correlations in the transition zone region. Ray and Anderson (1994) found good correlations between integrated slab locations since the breakup of Pangea and fast velocities in the depth range 220–1022 km. Wen and Anderson (1995) quantified the slab flux by estimating the subducted volume in the hotspot reference frame and correlated it with seismic tomography throughout the mantle. They found significant correlations in the depth interval 800–1100 km and attributed these to the accumulation of subducted lithosphere in this region. Correla-

* Corresponding author.

PII S0031-9201(96)03162-7

tions were also found in the upper mantle and transition zone for recent subduction.

The relationship between hotspots and seismic tomography has also been investigated. Excellent correlations at degree $l = 2$ were found in the lower mantle and at degree $l = 6$ in the upper mantle (Richards et al., 1988; Cazenave et al., 1989; Kedar et al., 1993). Cazenave et al. (1989) interpreted their results in terms of degree 2 convection in the lower mantle and degree 6 dominated convection in the upper mantle. Richards et al. (1988) hypothesized that hotspots originated in the deep lower mantle, based on the good correlations at degree 2, whereas Montagner and Romanowicz (1993) speculated that hotspots came from the transition zone, based on the dramatic decrease in the correlation below the transition zone, at degree 6.

One of the difficulties in relating tomography in the upper mantle with subduction and hotspots is the complexity and multiple causes of lateral velocity changes in this region. Large contributions from the cooling of the oceanic plates and cratonic 'roots' make it difficult to obtain meanful results from the hotspot and slab correlations with the seismic tomography. The role of deep cratonic 'roots' in the upper mantle has been extensively discussed (Lerner-Lam and Jordan, 1987; Hara and Geller, 1994; Polet and Anderson, 1995). The contribution from downgoing slabs, or possible stagnant slabs, may also prevent one from correctly relating seismic tomography to hotspots.

One can extract geodynamical information from seismological data in various ways. One method is to introduce an a priori regionalization of the upper mantle and use data to infer the parameters (e.g. Toksoz and Anderson, 1966; Nataf et al., 1986; Nataf and Ricard, 1996). Another way is to separate out the effects of near-surface features from the current generation of seismic tomographic models (e.g. Forte et al., 1995). Forte et al. (1995) decomposed seismic tomography into 'correlated' and 'uncorrelated' components with respect to the continent–ocean function, but other contributions may also be mapped into the 'correlated' component if these contributions are not totally 'uncorrelated' with the continent–ocean function. In this paper, recognizing problems of coverage, resolution and radial smearing, we test a current tomographic model for its geodynamic content, and we construct residual tomographic maps for the upper mantle by excluding effects of conductive cooling of oceanic plates, cratonic 'roots', and the cooling or partial melting associated with downgoing slabs. It is of interest to see if useful geodynamic information can be extracted from the current generation of seismic tomographic models. The residual tomography is compared with the pattern of subduction history in the past 130 Ma (Wen and Anderson, 1995) and with the distribution of hotspots. The procedures for excluding these effects are given in Section 2. The correlation between residual tomography and past subduction is presented in Section 3. The relationship between the distribution of hotspots and residual tomography and distribution of cratons is discussed in Section 4.

2. Residual upper-mantle tomographic models

The first-order contributors to seismic tomography in the upper mantle are assumed to be oceanic plates, cratonic 'roots', and continuing subduction. Other possible contributors, such as hotspots, stagnant slabs, and small-scale mantle convection are assumed to be second order. If they are important, they may show up in the residual maps. The residual tomography is defined as the seismic tomography excluding the effects of the first-order contributors. We use the seismic tomographic model SH12WM13 (Su et al., 1994).

2.1. Oceanic plates

Our first job is to remove from the tomographic models the effects of the cooling of oceanic plates. Velocity heterogeneities can be related to temperature variation of the mantle by the temperature derivatives for the minerals in the mantle. The temperature distribution beneath oceans can be calculated from the age of oceanic lithosphere and thermal cooling models (De Jonge et al., 1994; Nataf and Ricard, 1996). We use the digital age map of Müller et al. (1993).

Fig. 1 shows the velocity perturbation variation with the age of the oceanic lithosphere at depths from 100 to 650 km, based on the seismic tomo-

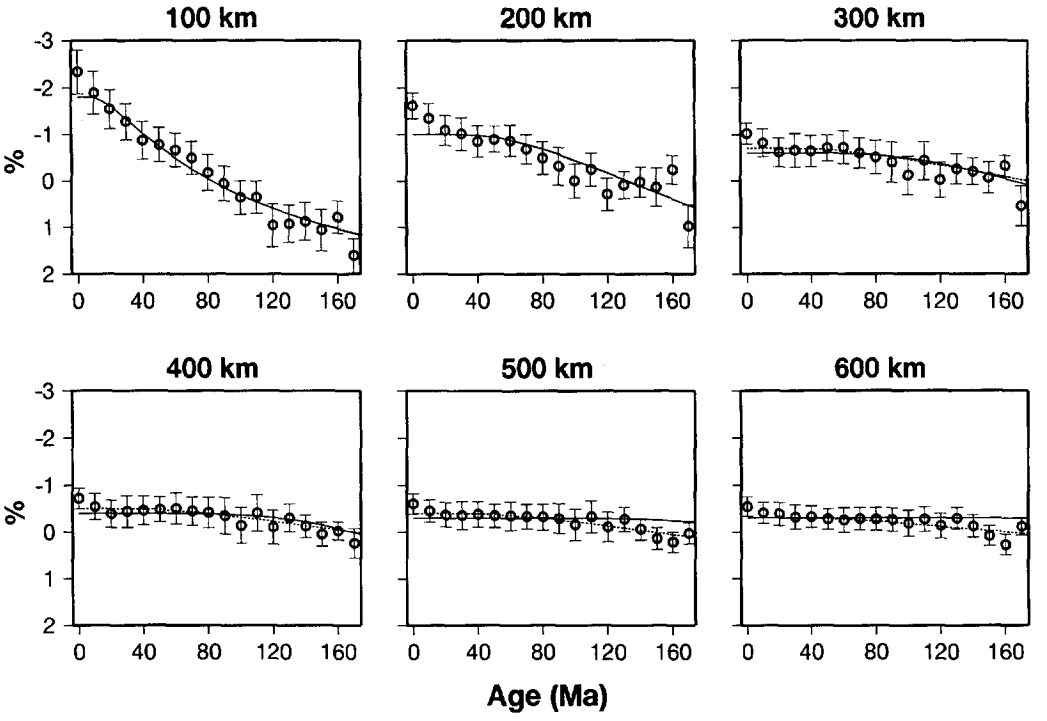

Fig. 1. The velocity perturbation vs. age of oceanic plates at various depths, based on SH12WM13 (Su et al., 1994) and digital age map (Müller et al., 1993). The velocity perturbations are averaged along each isochron. The r.m.s. values, based on SH12WM13, with respect to the mean velocities are also plotted.

graphic model SH12WM13 (Su et al., 1994) (circles). The velocity perturbations are calculated by averaging the velocity perturbations along the positions corresponding to each isochron on the surface of the earth. The velocity perturbation vs. age curves at different depths have the same characteristics; they are flat over a certain period of age, then increase with age. The 'turning points' of these curves are strongly dependent on the thermal diffusivity. However, with thermal diffusivity of $\kappa = 1.0\,\mathrm{mm^2\,s^{-1}}$, conduction is primarily confined to about the top 150 km of the mantle. There are two possible explanations for the observed relation of average velocities and age of oceanic plates: (1) if the tomographic models are 'exact' and do not suffer from any smearing, conductive cooling may extend deeper than general assumed; diffusivity changes, for example, owing to chemical changes with depth may be involved; (2) the current generation of seismic tomographic models have problems of resolution, coverage and crustal corrections. Details such as lithospheric thickening with age probably cannot be accurately recovered. The relation between velocity perturbations and age may be due to the smearing effects of the seismic inversion.

Our goal is to remove, empirically, the near-surface effects rather than interpreting them. We try two ways to remove the effects of the conductive cooling of oceanic plates:

1. A cooling model with one layer (0–210 km) with thermal diffusivity of $\kappa_1 = 1.65\,\mathrm{mm^2\,s^{-1}}$ (Kobayashi, 1974) over a half-space is used to explain the velocity–age curves at various depths. The effective diffusivity below 210 km is assumed to be $\kappa_2 = 3.3\,\mathrm{mm^2\,s^{-1}}$. There is still one unknown, the conductivity ratio between that of the layer and that of the half-space. The temperature derivatives which relate the temperature perturbation to velocity perturbation are uncertain (Estey and Douglas, 1986; Karato, 1993). Effects of pressure and chemical differences would make these parameters even more uncertain. As our

purpose is to find the best fit model, and remove it, rather than to find the conductivity ratio or temperature derivatives, we make no attempt to guess these parameters, but fix the conductivity ratio and find the best temperature derivatives at various depths. The best fit velocity models, in the oceanic regions, are found by adjusting the temperature derivatives, at various depths, so as to minimize the difference between the thermal velocity model and SH12WM13 in the oceanic regions. The predicted velocity–age relations are indicated as light lines in Fig. 1.

2. We assume that age-correlated variations in the mantle below 200 km are the result of smearing by the inversion. The theoretical temperature models are calculated by a half space cooling model ($\kappa = 1.65\,mm^2\,s^{-1}$) above 200 km. The theoretical temperature distribution below 200 km is assumed to be the same as that at 200 km predicted by the half-space cooling model (this can be thought of as equivalent to the 'smearing' effects in tomography). The best fit velocity models are found by the same procedure as in (1). The predicted velocity–age relations are indicated as dashed lines in Fig. 1.

The resultant residual tomographic models from both procedures are the same above 200 km and only slightly different between 200 and 400 km depths. The follow-up analysis, using the residual tomographic models, gives the same results. The high-velocity behavior under old lithosphere in the transition zone (400–670 km) could be due to the effect of stagnant slabs. For simplicity, we present the results by using the resultant residual tomographic models from Procedure 1. The predicted models are expanded into spherical harmonics and are truncated at degree 12, to compare with SH12WM13. The first residual tomography (RES1) is obtained by excluding the oceanic plate component from the seismic tomography (SH12WM13).

2.2. Cratons

The contribution of cratonic 'roots' to seismic velocity variation in spherical harmonic space is obtained by expanding the function, which, in cra-

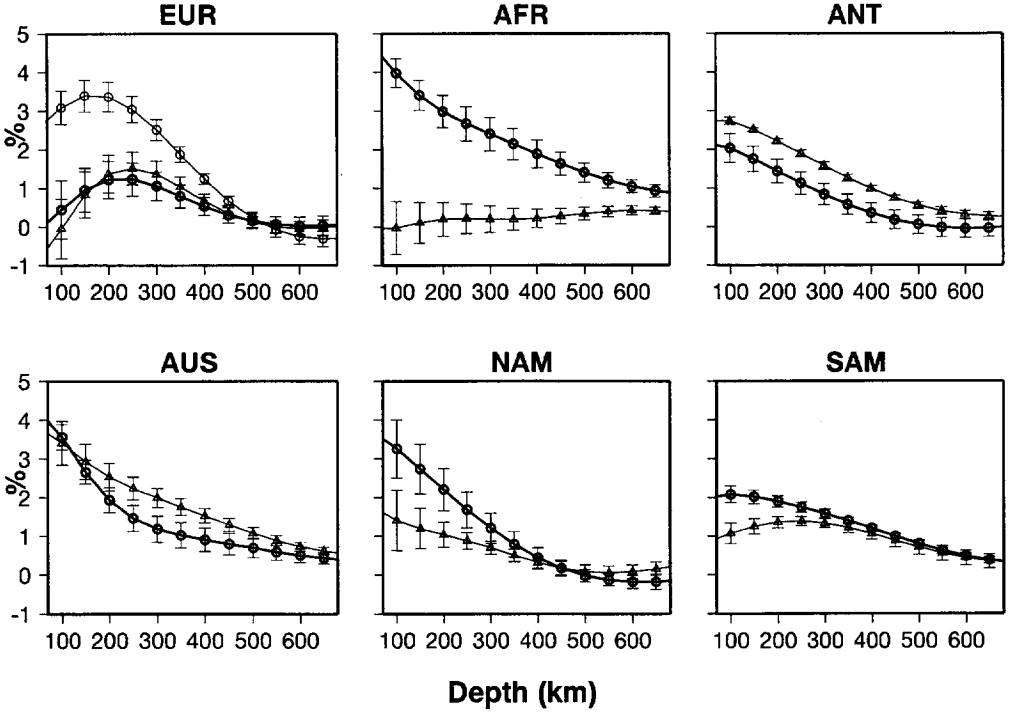

Fig. 2. The average velocity perturbations beneath each group of cratons vs. depth. The r.m.s. values, based on SH12WM13, with respect to the mean velocities are also plotted.

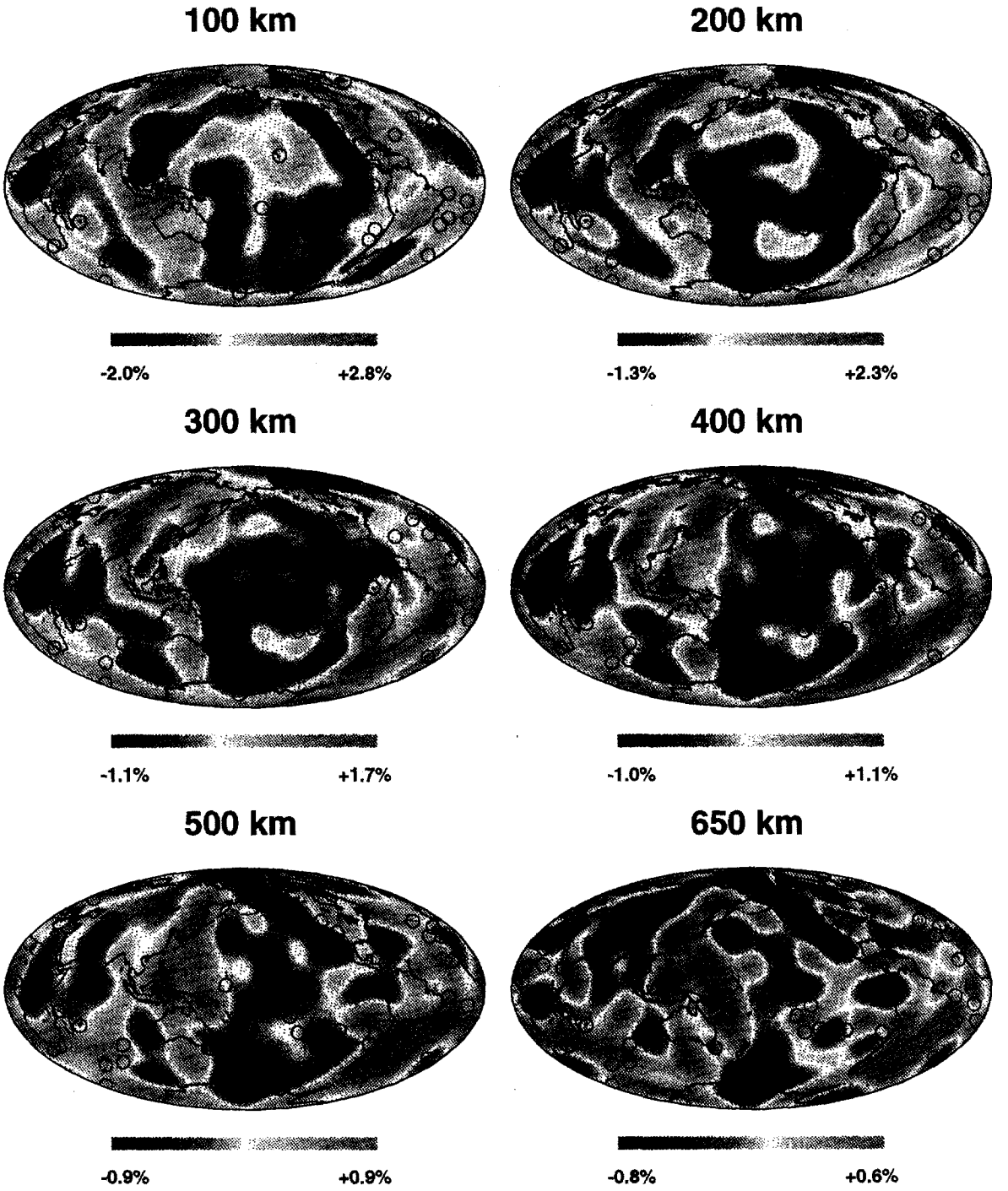

Fig. 3. Residual tomographic models at various depths in the upper mantle. The positions of hotspots are indicated by circles.

tonic regions, for each group of cratons, has the value of the average velocity perturbations from the residual tomography (RES1), and zero outside, into spherical harmonics. We classify the cratons according to their geographic locations and ages based on Sclater et al. (1981). The cratons are divided into 13 groups; six for cratons between 800 and 1700 Ma (Middle Proterozoic), and seven for those older than 1700 Ma (Archean and Early Proterozoic). Each group is related to a major plate. For instance, cratons between 800 and 1700 Ma on the South American plate are placed in the same group. Cratons older than 1700 Ma in Eurasia fall into two groups. Fig. 2 shows the velocity perturbations beneath each group of cratons vs. depth. The bold lines and circles are the velocity perturbations for cratons older than 1700 Ma. The light lines and triangles are for cratons between 800 and 1700 Ma. This set of spherical harmonic coefficients can be multiplied by an arbitrary constant (C). This proportionality constant (C) is a parameter to be determined later. The goal is to remove the direct effect of the cratons from mantle tomography.

2.3. Continuing subduction

We assume that the subducting plates sink vertically into the upper mantle at the velocity of the plate at the trench. The ages of the slabs are reconstructed at every depth. We assume that the seismic velocity perturbation within the slab is constant (δV_s) at a certain depth. The width of a particular slab segment is equal to its thickness. Thickness is calculated from the age of the oceanic lithosphere at the time of subduction (Wen and Anderson, 1995). Continuing subduction can cause low velocities in the shallow mantle, because of volatile fluxed melting in the mantle wedge (Anderson et al., 1992), and high velocities at greater depth, owing to low temperatures in the slab. We permit δV_s to take on negative or positive values (negative values imply partial melting).

2.4. Residual tomographic models

Synthetic models are obtained by linear superposition of the contributions from slabs, oceanic plates, and cratons at various depths. The two parameters (δV_s and C) at each depth are chosen by minimizing the quantity

$$\Sigma\sqrt{V_{syn}^2 - V_{tomo}^2}$$

where V_{syn} and V_{tomo} are the velocity perturbations of the synthetic model and SH12WM13, at a certain depth, respectively. The summation is over every $1° \times 1°$ cell in a global grid. The residual models are obtained by subtracting synthetic tomography from SH12WM13. The residual models for 100–650 km depths are plotted in Fig. 3. It should be noted that the possible effects of Gibbs oscillations owing to the spherical harmonic truncations may influence our

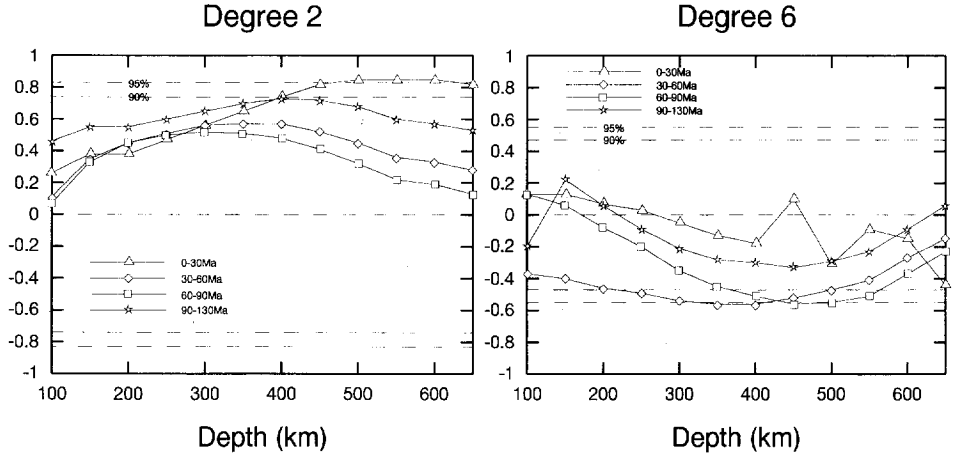

Fig. 4. Correlation coefficients between the residual tomography and subduction history, at degree $l = 2$ and 6.

result to some extent, even though they are second order compared with the uncertainties in the subtraction of oceanic lithospheric cooling.

3. Correlations between residual tomographic models and subduction history

No significant correlations are found between residual tomography and subduction history between 30 and 130 Ma (Wen and Anderson, 1995) (see Fig. 4). There are some negative correlations between 30–90 Ma subduction and residual tomography in the 350–500 depth range. Residual tomography correlates with 0–30 Ma subduction, only at degree $l = 2$, with high velocities corresponding to regions of subduction in the transition zone region. Correlations are less pronounced for the resultant residual tomography model by Procedure 2. The correlations appear to be due to the high velocities beneath several subduction zones (e.g. Kurile, Japan, Izu–Bonin, Mariana, New Hebrides and Philippine trenchs, i.e. the western Pacific, generally west-dipping slabs) rather than the global subduction pattern. We test this possibility by dividing the subduction in the past 30 Ma into two groups. Group 1 contains only the 0–30 Ma subduction in the Kurile, Japan, Izu–Bonin, Mariana, New Hebrides and Philippine trenches; Group 2 includes subduction in the other convergence regions (e.g. Aleutian, Chile–Peru, Tonga–Fiji, Java trenches, etc). We found excellent correlations at degree 2 and 3 for Group 1 subduction and no correlation for Group 2 subduction (Table 1). Correlations which are significant at greater than 90% confidence level are underlined. The correlations have two possible explanations:

1. The resolution of the seismic model prevents us from excluding the existing slabs efficiently by introducing the theoretical slab function. If slabs in the transition zone beneath the Group 2 subduction zones were not recovered in the seismic inversion, perhaps because of coverage problems, we cannot exclude efficiently the effects of con-

Table 1
Correlations between 0–30 Ma subduction and residual tomography

Depth (km)	Degree 1 = 2		Degree 1 = 3	
	Group 1	Group 2	Group 1	Group 2
400	0.60	0.03	0.12	−0.70
450	0.74	−0.06	0.39	−0.80
500	0.83	−0.15	0.58	−0.83
550	0.88	−0.20	0.64	−0.84
600	0.91	−0.20	0.71	−0.80
650	0.91	−0.26	0.67	−0.81

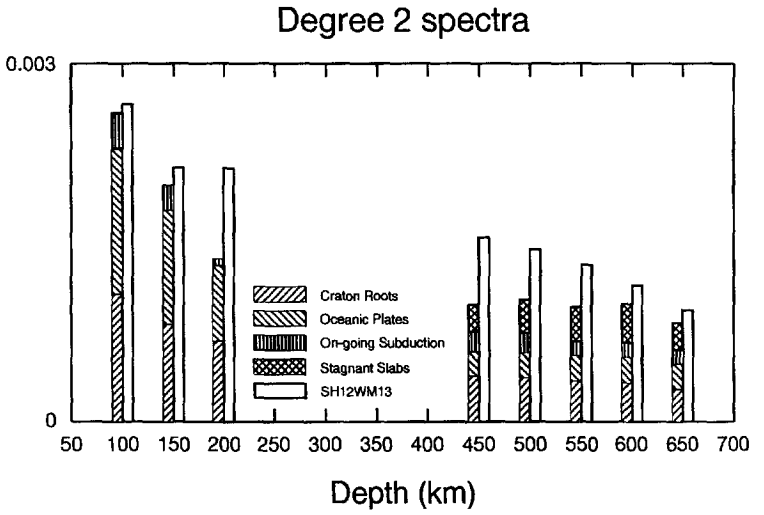

Fig. 5. The degree 2 power spectra of SH12WM13, cratonic 'roots', continuing subduction, oceanic plates, and stagnant slabs in the upper mantle.

tinuing subduction from our procedures. We cannot discard this possibility for the present generation of tomographic models.

2. Some slabs beneath Group 1 trenches accumulate in the transition zone region for a period of time. The behavior of the slab at the 670 km discontinuity is region dependent, as suggested by seismology (e.g. Jordan and Lynn, 1974; Zhou and Anderson, 1989; Van der Hilst et al., 1991; Fukao et al., 1992) and geodynamics (Gurnis and Zhong, 1995). It may also be true that other effects, such as slab dip, direction of dip, trench migration or presence of back-arc basins are important and that the distinction between Group 1 and Group 2 slabs is geodynamically significant.

The degree 2 heterogeneity is the most important component for many geophysical observables, such as seismic velocity (e.g. Masters et al., 1982) and geoid (Lerch et al., 1979). However, the origin of this degree is still controversial. For the analysis of the power spectrum, we interpret the high velocities beneath Group 1 trenches as stagnant slabs and subtract their effect from the residual tomography in the transition zone (450–650 km), assuming that stagnant slabs are only beneath Group 1 trenches. Fig. 5 shows the power spectra of the seismic tomography (SH12WM13), cratonic roots, current subduction and stagnant slabs, at degree $l = 2$. In the shallow mantle (above 200 km), the oceanic lithosphere, cratons and subducting slabs contribute most of the power at degree 2. In the transition zone, stagnant slabs are also responsible for the degree 2 lateral variation.

4. Hotspots, cratons and mantle convection

Residual tomography, which excludes the near-surface features, may provide a constraint on convection in the mantle. Passive ridges are the first-order upwellings on the surface of the Earth. They possibly represent normal (uncooled) mantle. Hotspots are generally considered to be caused by deep, narrow, active upwellings. In this section, we use seismic tomography to attempt to constrain the characteristics of hotspots throughout the mantle. We use seismic tomography (SH12WM13) in the lower mantle and residual tomography in the upper mantle. The list of 47 hotspots, compiled by Morgan (1981) and Crough and Jurdy (1980), is used.

The overall distribution of hotspots correlates very well with low seismic velocities in the deep lower mantle (1700 km; core–mantle boundary (CMB)) at degree $l = 2$. There is some correlation with degree $l = 3$ as well in the lower mantle. However, the degree 2 correlations are poor in the depth region 700–1700 km (except 900–1000 km). This is consistent with the results of previous workers (e.g. Kedar et al., 1993). Table 2 gives correlation coefficients between hotspot distribution and residual tomography in the upper mantle. Positive values mean that hotspot positions favor low-velocity regions. Correlations which are significant at the greater that 90% confidence level are underlined. Hotspots correlate with slow seismic velocities at degree $l = 2$ to 400 km depth and at degree $l = 4$ to 150 km depth. The degree 2 correlations decrease very rapidly into the transition zone. Also, at degree $l = 4$, hotspots correlate with fast velocities in part of the transition region (400–500 km) (Table 2). There is no significant correlation at degree $l = 6$ between hotspot distribution and residual tomography in the upper mantle.

It is useful to discuss hotspots in the context of the three-dimensional residual velocity structure of the upper mantle. Most of the hotspots in the Pacific and circum-Pacific area are in long-wavelength low-velocity regions of the upper mantle. Some hotspots

Table 2
Correlations between hotspots and residual tomography at degree l = 1 to l = 6

Depth (km)	Degree					
	1	2	3	4	5	6
100	−0.42	0.47	0.17	0.90	−0.03	0.36
150	−0.47	0.79	0.19	0.72	−0.01	0.44
200	−0.62	0.86	0.11	0.43	−0.03	0.47
250	−0.70	0.85	0.04	0.09	−0.04	0.45
300	−0.80	0.83	−0.17	−0.23	−0.04	0.40
350	−0.84	0.77	−0.34	−0.54	−0.03	0.03
400	−0.89	0.76	−0.46	−0.72	−0.01	0.26
450	−0.82	0.53	−0.56	−0.87	−0.08	0.36
500	−0.75	0.39	−0.48	−0.80	0.13	0.40
550	−0.64	0.23	−0.43	−0.71	−0.15	0.43
600	−0.42	0.15	−0.33	−0.68	−0.16	0.46
650	−0.32	0.08	−0.27	−0.60	−0.05	0.44

are also in low-velocity regions in Africa, the Indian Ocean and the North Atlantic. Most hotspots in the South Atlantic, around South America and near South Africa are in high-velocity regions. The occurrence of high velocities under some hotspots in Africa could be because they are close to high-velocity cratonic 'roots'. This spatial visual check and the good correlations at degree $l = 4$ suggest that correlations between hotspot and residual seismic tomography in the upper 400 km, at long wavelengths, are meaningful (Table 2).

Is there any connection between the correlations at shallow depths and lowermost mantle? No significant correlation is found between seismic tomography at 2500 km and residual tomographic models, at degree $l = 2$ (Fig. 6). The correlation is negative for residual tomography at 650 km. Tomographic models from 1700 km to the CMB have similar correlations. However, residual tomographic models between 200 and 500 km depth correlate with the seismic tomography model in the 900–1000 km depth region. This is the only region in the lower mantle that correlates with residual tomography. Direct comparison among the degree 2 patterns of hotspots, residual tomography and lower-mantle tomography is shown in Fig. 7. They all have low values in the central Pacific and Africa; the residual tomography and hotspot highs (devoid of hotspots) extend to the south of South America and east of Asia. It is not clear how to relate the correlations at shallow depths with those in the deep mantle. However, it does appear that degree 2 is one of the fundamental modes in mantle convection. This is not predicted by convection models with uniform boundary conditions (e.g. Tackley et al., 1993). Hotspots do not appear to originate in mantle that has been cooled or blocked by slab. Previously normal mantle which has been cooled by subduction (fast seismic velocities) will, of course, correlate with subduction history. However, tomography in this mantle will also correlate with hotspots, even if only 'normal' mantle is present. Downwellings in the deep lower mantle, whether they are caused by slab accumulations or are indirectly related to present or past subduction, will make the seismic patterns in this region correlate with hotspots. Do slabs cool the mantle or do plumes heat the mantle, or both? Is 'normal' mantle uncooled or not heated? The cause and the effect must still be disentangled.

The degree $l = 6$ correlation between upper-mantle tomography and distribution of hotspots is actually a representation of correlation of distribution of cratons and distribution of hotspots at this degree. Fig. 8 shows the degree 6 map of the craton function, which has unit value in cratonic regions and zero outside. The degree $l = 6$ expansion has highs in most of the cratonic regions and lows in the North

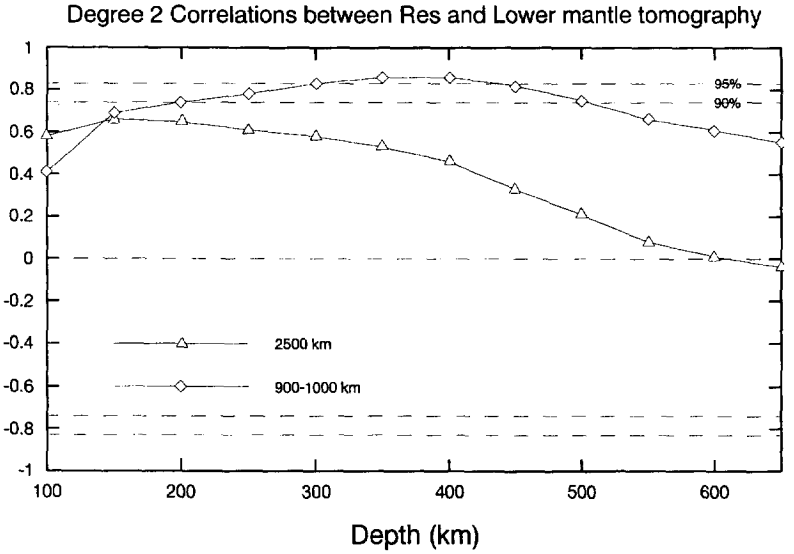

Fig. 6. Correlations between the residual tomographic models and seismic tomographic model at 2500 km and 900–1000 km depths.

Hotspot Density: degree 2

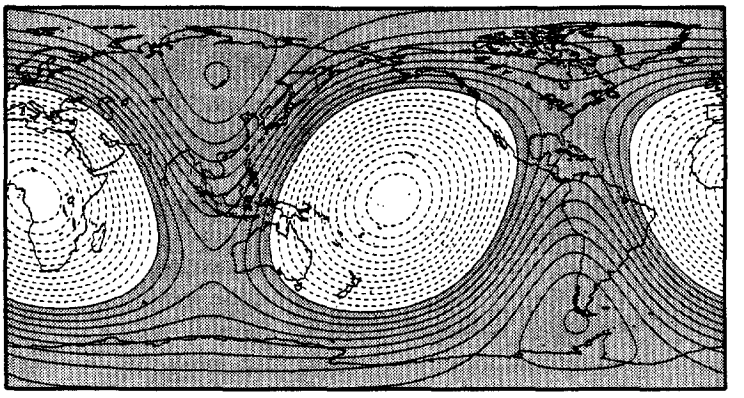

Residual Tomography (300 km): degree 2

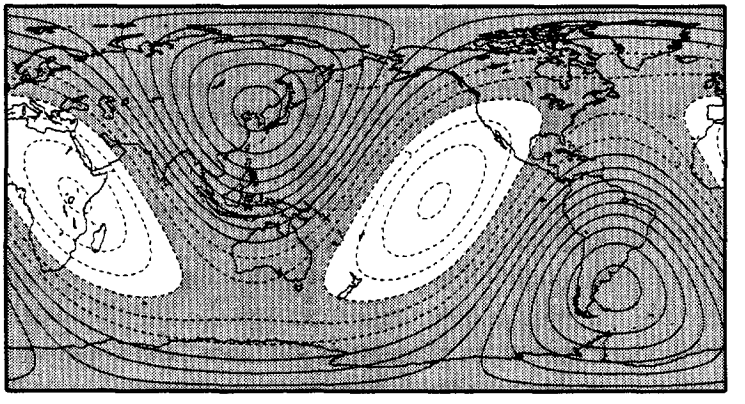

SH12WM13 (2500 km): degree 2

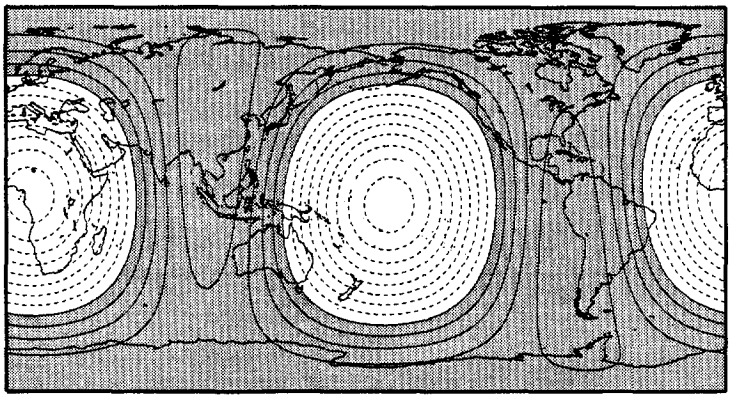

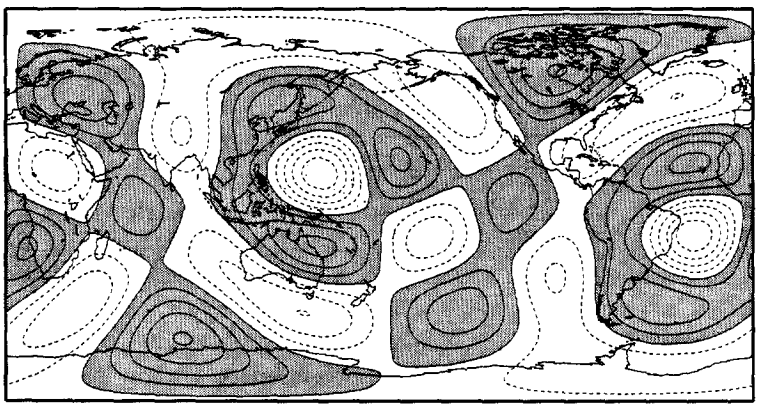

Fig. 8. Degree 6 pattern of craton function, which has unit value in cratonic regions and zero outside. The dashed-contour area indicates the places with low numbers of cratons.

Atlantic, equatorial Atlantic, the Pacific superswell, south of New Zealand and the Afar. It looks very much like the degree $l = 6$ hotspot (Cazenave et al., 1989) and dynamic topographic maps (Cazenave and Thoraval, 1994).

This has several possible explanations:

1. the pattern of convection in the upper mantle is modulated by cratons; hot upwellings occur in complementary locations. Cratons act as cold fingers and perturb the thermal and geometric properties of the boundary layer.
2. Hot upwelling mantle tends to drive cratons away and they settle in areas of colder mantle. Surface plates respond passively to mantle flow.
3. The degree $l = 6$ pattern of surface dynamic topography could be the result of hot upwellings, if cratonic 'roots' have normal densities, or the result of dense cratonic 'roots', or both.
4. Degree $l = 6$ convection is intrinsic to the upper mantle (Tackley et al., 1993). Cratons in cold regions and upwellings in complementary regions establish the phase of the pattern.

Thermal instability of the lower thermal boundary layer is unlikely to be the main control on mantle convection. Cratons probably have long-lived 'roots' extending to about 200 km, and associated cold, high-velocity material may extend somewhat deeper. This is a large fraction of the depth of the upper mantle and the presence of thick cratons must influence mantle convection. In addition, a moving craton overrides cold oceanic lithosphere, placing a cold slab about 100 km thick under the craton. This cold dense downwelling also affects mantle convection, even after it settles 'on the bottom'. The upper mantle could be a system, cooled and dragged down at subduction zones and affected by lateral temperature gradients at the surface, with subcratonic isotherms at a deeper level than isotherms elsewhere, except in slabs. This general type of convection was treated by Pekeris (1935), Allan et al. (1967) and King and Anderson (1995). It is distinct from the Rayleigh–Bénard convection in a fluid system heated from below which forms the basis for most discussions of mantle convection. The mantle could be heated from below and from within and could also be cooled from below.

Much attention has been focused at degrees $l = 2$ and $l = 6$ (e.g. Richards et al., 1988; Cazenave et al., 1989). Convection in a spherical shell with phase changes or an increase of viscosity with depth gives

Fig. 7. Degree 2 patterns for hotspot distribution, residual tomography at 300 km and seismic tomography at 2500 km. The dashed-contour area indicates the places with high numbers of hotspots or low seismic velocities.

a red spectrum with spectral peaks between degrees $l = 2$ and $l = 6$ (Bunge et al., 1996). It has long been known that surface boundary conditions may act as a template for convection (e.g. Pekeris, 1935; Elsasser, 1969). The degree $l = 6$ pattern of hotspots has been attributed to a natural scale of plume formation (Richards et al., 1988) and a characteristic of the lower thermal boundary. However the strong degree $l = 6$ convection could be intrinsic to the background flow, modulated by subduction history and surface boundary conditions.

5. Conclusion

Residual tomography is calculated from seismic tomography by excluding the effects of oceanic lithosphere cooling, cratonic 'roots' and cooling or partial melting associated with subducted slabs in the upper mantle. There is no correlation between 30–30 Ma subduction and residual tomography in the upper mantle. Residual tomography in the transition zone correlates with 0–30 Ma subduction, especially the subduction in the Kurile, Japan, Izu–Bonin, Mariana, New Hebrides and Philippine trenchs. This can be explained either by stagnant slabs beneath those trenches or by lack of lateral resolution of seismic tomography in other subduction regions. Most (slightly more than half) hotspots appear to be in slow regions of the upper mantle. The overall pattern of hotspots correlates with residual tomography in the top 400 km at degree $l = 2$ and 4. Correlations decrease very rapidly in the transition zone region. About 25% of the hotspots occur in regions of the mantle which are slow down to 650 km depth. Hotspots also correlate with seismic tomography in the 900–1000 km region and the deep lower mantle at spherical harmonic degree $l = 2$. However, the correlation between residual tomography in the upper mantle and seismic tomography in the deep lower mantle is poor. At spherical harmonic degree $l = 6$, the distribution of hotspots correlates with the distribution of cratons and residual topography instead of residual tomography. Cratons may affect the locations of upwellings, thus modulating mantle convection, or the degree $l = 6$ could be intrinsic with cratons and hotspots establishing the pattern. Mantle convection could be a system controlled by subduction and modulated by near-surface conditions (Elsasser, 1969).

Acknowledgements

We thank Jascha Polet for providing digital data of cratons. This work was funded by NSF Grant EAR 92-18390. This paper is Contribution 5554 of the Division of Geological and Planetary Sciences, California Institute of Technology.

References

Allan, D.W., Thompson, W.B. and Weiss, N.O., 1967. Convection in the Earth's mantle. In: S.K. Runcorn (Editor), Mantles of the Earth and Terrestrial Planets. Interscience, London, pp. 507–512.

Anderson, D.L., Tanimoto, T. and Zhang, Y.-S., 1992. Plate tectonics and hotspots: the third dimension. Science, 256: 1645–1651.

Bunge, H.-P., Richards, M.A. and Baumgardner, J.R., 1996. Effect of depth-dependent viscosity at the platform of mantle convection. Nature, 379: 436–438.

Cazenave, A. and Thoraval, C., 1994. Mantle dynamics constrained by degree 6 surface topography, seismic tomography and geoid: inference on the origin of the South Pacific Superswell. Earth Planet. Sci. Lett., 122: 207–219.

Cazenave, A., Souriau, A. and Dominh, K., 1989. Global coupling of Earth surface topography with hotspots, geoid and mantle heterogeneities. Nature, 340: 54–57.

Crough, S.T. and Jurdy, D.M., 1980. Subducted lithosphere, hotspots and the geoid. Earth Planet. Sci. Lett., 48: 15–22.

De Jonge, M.R., Wortel, M.J.R. and Spakman, W., 1994. Regional scale tectonic evolution and the seismic velocity structure of the lithosphere and the upper mantle: the Mediterranean region. J. Geophys. Res., 99: 12091–12108.

Elsasser, W.M., 1969. Convection and stress propagation in the upper mantle. In: S.K. Runcorn (Editor), The Application of Modern Physics to the Earth and Planetary Interiors. Wiley–Interscience, New York.

Estey, L.H. and Douglas, B.J., 1986. Upper mantle anisotropy: a preliminary model. J. Geophys. Res., 91: 11393–11406.

Forte, A.M., Dziewonski, A.M. and O'Connell, R.J., 1995. Continent–ocean chemical heterogeneity in the mantle based on seismic tomography. Science, 268: 386–388.

Fukao, Y., Obayashi, M., Inoue, H. and Nenbai, M., 1992. Subducting slabs stagnant in the mantle transition zone. J. Geophys. Res., 97: 4809–4822.

Gurnis, M. and Zhong, S., 1995. Dynamic influences of plates with faulted and mobile margins on slab penetration through the 670-km phase change. (Abstract) EOS Trans. Am. Geophys. Union, Spring Meeting Suppl., 76(17): S57.

Hara, T. and Geller, R., 1994. The geological origin of long wavelength lateral heterogeneity at depths of 300–400 km. Geophys. Res. Lett., 21: 907–910.

Jordan, T.H. and Lynn, W.S., 1974. A velocity anomaly in the lower mantle. J. Geophys Res., 79: 2679–2685.

Karato, S., 1993. Importance of anelasticity in the interpretation of seismic tomography. Geophys. Res. Lett., 20: 1623–1626.

Kedar, S., Anderson, D.L. and Stevenson, D.J., 1993. Relationship between hotspots and mantle structure: correlation with whole mantle seismic tomography. In: D.B. Stone and S.K. Runcorn (Editors), Proceedings of the NATO Advanced Study Institute on Dynamic Modeling and Flow in the Earth and Planets. Kluwer Academic, Dordrecht, pp. 249–259.

King, S.D. and Anderson, D.L., 1995. An alternative mechanism of flood basalt formation. Earth Planet. Sci. Lett., 136: 269–279.

Kobayashi, Y., 1974. Anisotropy of thermal diffusivity in olivine, pyroxene and dunite. J. Phys. Earth, 22: 359–373.

Lerch, F.J., Klosko, S.M., Laubscher R.E. and Wagner, C.A., 1979. Gravity improvement using GEOS3 (GEM9 and 10). J. Geophys. Res., 84: 3897–3916.

Lerner-Lam, A.L. and Jordan, T.H., 1987. How thick are the continents? J. Geophys. Res., 92: 14007–14026.

Masters, G., Jordan, T.H., Silver, P.G. and Gilbert, F., 1982. Aspherical Earth structure from fundamental spheroidal-mode data. Nature, 298: 609–613.

Montagner, J.-P. and Romanowicz, B., 1993. Degree 2, 4, 6 inferred from seismic tomography. Geophys. Res. Lett., 20: 631–634.

Morgan, W.J., 1981. Hotspot tracks and the opening of the Atlantic and Indian oceans. In: C. Emiliani (Editor), The Sea. Wiley–Interscience, New York, pp. 443–487.

Müller, R.D., Roest, W.R., Royer, J.-Y., Gahagan, L.M. and Sclater, J.G., 1993. A digital age map of the ocean floor. SID Reference Series, Scripps Institution of Oceanography, University of California, La Jolla, CA, 93-303.

Nataf, H.-C. and Ricard, Y., 1996. 3SMAC: An a priori tomographic model of the upper mantle based on geophysical modeling. Phys. Earth Planet. Inter., 95: 101–122.

Nataf, H.-C., Nakanishi, I. and Anderson, D.L., 1986. Upper mantle heterogeneity and anisotropy. J. Geophys. Res., 91: 7261–7307.

Pekeris, C.L., 1935. Thermal convection in the interior of the Earth. Mon. Not. R. Astron. Soc., Geophys. Suppl., 3: 343–367.

Polet, J. and Anderson, D.L., 1995. Depth extent of cratons as inferred from tomographic studies. Geology, 23: 205–208.

Ray, T.W. and Anderson, D.L., 1994. Spherical disharmonics in the Earth sciences and spatial solution: ridges, hotspots, slabs, geochemistry and tomography correlations. J. Geophys. Res., 99: 9605–9614.

Richards, M.A. and Engebretson, D.C., 1992. Large-scale mantle convection and the history of subduction. Nature, 335: 437–440.

Richards, M.A., Hager, B.H. and Sleep, N.H., 1988. Dynamically supported geoid highs over hotspots: observation and theory. J. Geophys. Res., 93: 7690–7708.

Sclater, J.G., Parsons, B. and Jaupart, C., 1981. Oceans and continents: similarities and differences in the mechanisms of heat loss. J. Geophys. Res., 86: 11535–11552.

Scrivner, C. and Anderson, D.L., 1992. The effect of post Pangea subduction of global mantle tomography and convection. Geophys. Res. Lett., 19: 1053–1056.

Su, W.-J., Woodward, R.L. and Dziewonski, A.M., 1994. Degree 12 model of shear velocity heterogeneity in the mantle. J. Geophys. Res., 99: 6945–6980.

Tackley, P.J., Stevenson, D.J., Glatzmaier, G.A. and Schubert, G., 1993. Effects of an endothermic phase transition at 670 km depth in a spherical model of convection in the Earth's mantle. Nature, 361: 699–704.

Toksoz, M.N. and Anderson, D.L., 1966. Phase velocities of long-period surface waves and structure of the upper mantle. J. Geophys. Res., 71: 1649–1658.

Van der Hilst, R., Engdahl, R., Spakman, W. and Nolet, N., 1991. Tomographic imaging of subducted lithosphere below northwest Pacific island arcs. Nature, 353: 37–43.

Wen, L. and Anderson, D.L., 1995. The fate of slabs inferred from seismic tomography and 130 million years of subduction. Earth Planet. Sci. Lett., 133: 185–198.

Zhou, H.-W. and Anderson, D.L., 1989. Search for deep slabs in the northwest Pacific mantle. Proc. Natl. Acad. Sci. USA, 86: 8602–8606.